Chapter 6
Neoclassical Modeling of Bias Induced Plasma Flows

6.0 Introduction

In order to predict the evolution of the plasma flows and electric fields subject to the biased electrode, it is necessary to model the behavior of the plasma subject to the **j**x**B** force of the electrode return current. In this work, a purely neoclassical model of the plasma will be used. The continuity and momentum equations are solved to yield the radial conductivity, flow directions, and time scales for plasma flow evolution. The damping mechanisms used include linear neoclassical parallel viscosity and ion-neutral friction. Two models for the time evolution of the flows are presented, corresponding to the plasma response to the turn on and turn off of the electrode.

Section 1 will lay out the fluid equations and provide the steady state solution for the plasma flows and radial conductivity. Section 2 provides a review of the calculation of the viscosity coefficients. Section 3 provides more details of the neutral particle physics and modeling. Section 4 details the two separate time dependent solution of the fluid equations for the spin-up and relaxation of the plasma flows. Section 5 presents a brief comparison of the viscous damping in the QHS and 10% Mirror configurations.

A note on units is appropriate at this juncture. All equations are written in the CGS system, so that charge is measured in statCoulombs (1 statCoulomb = 3.3356×10^{-10} coulombs), potentials in statVolts or statCoulombs/cm (1 statVolt = 299.79 volts), flow velocity in cm/sec., energies in ergs, and pressures in ergs/cm^3. Electric fields are measured in statVolts/cm or statCoulombs/cm^2. Magnetic fields are measured in Gauss, although they also have the same units as electric fields. Magnetic flux has units of statCoulombs or statVolt·cm. Current density is measured in statCoulombs/cm^2·sec, so that conductivity has units of 1/sec. The units of various quantities in the modeling will be noted where appropriate.

6.1: Steady State Solutions to the Fluid Equations.

The development in this section will follow the method given by Coronado and Talmadge.[1] The derivation begins with the momentum balance and continuity equations for a given species a:

$$\begin{aligned} m_a N_a \frac{\partial}{\partial t}\mathbf{U}_a + m_a N_a (\mathbf{U}_a \cdot \nabla)\mathbf{U}_a &= e_a N_a\left(\mathbf{E} + \frac{\mathbf{U}_a \times \mathbf{B}}{c}\right) - \nabla p_a \\ &- \nabla \cdot \mathbf{D}_a - m_a N_a \upsilon_{an}\mathbf{U}_a + \mathbf{F}_a \end{aligned} \tag{6.1}$$

$$\frac{\partial}{\partial t}N_a + \nabla \cdot N_a \mathbf{U}_a = 0\,. \tag{6.2}$$

N_a is the number density of species a, $\mathbf{U}_a$ is the flow velocity, p_a is the scalar pressure, ν_{an} is the collision frequency between (assumed stationary) neutrals and species a, $\mathbf{F}_a$ is a friction force between species a and other plasma species, $\mathbf{\Pi}_a$ is the viscosity tensor, and m_a is the mass of a particle of species a.

Some modifications are made in this derivation compared to the original derivation in Coronado and Talmadge. The Hamada toroidal angle (ζ) and poloidal angle (α) are allowed to vary from 0 to 2π, instead of 0 to 1 in the original work. The expressions are written in terms of a general radial variable instead of the volume; the Jacobian ($\sqrt{g}$) is a flux surface constant which is left arbitrary for the moment.

The term $-m_a N_a \nu_{an} U_a$ represents momentum loss due to collisions with neutrals, and will be discussed in more detail below and in Appendix 3. In order to terminate the sequence of fluid equations, the heat flux is neglected by setting ∇T_i=0. The exchange of momentum between the electron and ion fluids is represented through the friction force

$$\mathbf{F}_i = m_i N_i \upsilon_{ie}(\mathbf{U}_e - \mathbf{U}_i), \tag{6.3}$$

with F_e=-F_i by momentum conservation. For the viscosities, we use the linear parallel neoclassical viscosity, as will be discussed in Section 6.2.

These moment equations will be expanded in the standard small gyroradius assumption, i.e. ε_a=$r_{L,a}$/L, where L is the scale length of the system. For HSX, the typical electron gyroradius is ≈0.1mm, while the ion gyroradius is ≈1mm. Typical scale lengths are a few centimeters in the radial direction, implying that the small gyroradius assumption is easily satisfied for both species. Furthermore, it is assumed that $U_a/v_{th,a}\sim O(\varepsilon_a)$ with $U_a\sim E_{\mathbf{ExB}}=E_r/B$, where $v_{th,a}$ is the thermal velocity of species a. We consider $\nu_{ie}/\omega_{ci}\sim O(\varepsilon_a)$, where ω_{ci} is the ion gyrofrequency, as well as $\nu_{in}/\omega_{ci}\sim O(\varepsilon_a)$. We also take $[(1/U_i)(\partial U_i/\partial t)]/\omega_{ci}\sim O(\varepsilon_a)$, along with $(\partial N_a/\partial t)/(\nabla\cdot N_a U_a)\sim O(\varepsilon_a)$.

With these scalings, the various terms in the momentum balance can be ordered as follows[2]

$$\frac{E}{\mathbf{U}_a \times \mathbf{B}} \approx \frac{U_{ExB}}{U_a} \approx O(\varepsilon^0)$$

$$\frac{N_a e_a \mathbf{E}}{\nabla p_a} \approx \frac{L_a n_a e_a E}{n_a T_a} \approx \frac{E}{B}\frac{L_a}{\omega_{ca} r_{La}^2} \approx O(\varepsilon^0)$$

$$\frac{m_a N_a (\mathbf{U}_a \cdot \nabla)\mathbf{U}_a}{N_a e_a \mathbf{E}} \approx \frac{m_a}{e_a B}\frac{B}{E}\frac{U}{L}U \approx \frac{L_a n_a e_a E}{n_a T_a} \approx \frac{r_{La}}{L}\frac{U}{v_{th,a}} \approx O(\varepsilon^2)$$

$$\frac{m_a N_a \upsilon_{ie}(\mathbf{U}_i - \mathbf{U}_e)}{e_a N_a \mathbf{E}} \approx \frac{m_a}{e_a B}\frac{B}{E}\upsilon_{ie} U \approx \frac{\upsilon_{ie}}{\omega_{ca}} \approx O(\varepsilon^1)$$

$$\frac{\nabla \cdot \mathbf{D}_a}{\nabla p_a} \approx \frac{\nabla n_a T_a \tau_a \nabla U_a}{\nabla n_a T} \approx \frac{U_a}{L\upsilon_i} \approx O(\varepsilon^1)$$

With this ordering of terms, the lowest (0^{th}) order momentum balance is simply given by radial force balance

$$eN_a\left(\mathbf{E} + \tfrac{1}{c}\mathbf{U}_a \times \mathbf{B}\right) = \nabla p_a, \tag{6.4}$$

and the lowest order continuity equation becomes

$$\nabla \cdot N_a \mathbf{U}_a = 0 . \tag{6.5}$$

Assuming that radial flows can be neglected and that the density is finite, this expression implies that the plasma flow is incompressible ($\nabla \cdot \mathbf{U}=0$). When incompressibility is coupled to the lowest order momentum balance, it is found that the contravariant poloidal and toroidal flows can be written[3]

$$U^{\alpha} = \frac{c}{B^{\zeta}\sqrt{g}}\left(\frac{\partial \Phi}{\partial \rho} + \frac{1}{eN_i}\frac{\partial p_i}{\partial \rho}\right) + \lambda B^{\alpha} \tag{6.6}$$

$$U^{\zeta} = \lambda B^{\zeta} . \tag{6.7}$$

In this equation, ρ is an arbitrary flux surface label, Φ is the potential, B^{ζ} is the contravariant toroidal magnetic field, B^{α} is the contravariant poloidal magnetic field, B and λ is the force free component of the parallel flow. This constant λ is equivalent to the bootstrap component of the flow, and is a function of ρ and time only. These two equations allow the contravariant flows to be related to the force free flow and the potential gradient, or vice versa, and will be used repeatedly. In Hamada coordinates, the **E**×**B** and diamagnetic flows, *and* the return flows to maintain incompressibility, are all contained in a single term in the expression for the poloidal flow. A detailed derivation of a similar pair of equations was given in Section 5.4.4, in the context of deriving the Pfirsch-Schlueter current. Note that λ has units of cm^2/(statVolt·sec).

The first order momentum balance equation can be written for ions as

$$\begin{aligned} m_i N_i^{(0)} \frac{\partial}{\partial t}\mathbf{U}_i^{(0)} &= eN_i^{(1)}\left(\mathbf{E}^{(0)} + \frac{1}{c}\mathbf{U}_i^{(0)} \times \mathbf{B}^{(0)}\right) + \\ & eN_i^{(0)}\left(\mathbf{E}^{(1)} + \frac{1}{c}\mathbf{U}_i^{(1)} \times \mathbf{B}^{(0)} + \frac{1}{c}\mathbf{U}_i^{(0)} \times \mathbf{B}^{(1)}\right) - \nabla p_i^{(1)} - \nabla \cdot \mathbf{D}^{(0)} - \\ & m_i N_i \upsilon_{in} \mathbf{U}_i^{(0)} - m_i N_i \upsilon_{ie}\left(\mathbf{U}_i^{(0)} - \mathbf{U}_e^{(0)}\right) \end{aligned} \tag{6.8}$$

The inertial term is second order, as shown above, and hence neglected. The first order momentum balance for electrons is written as

$$
\begin{gathered}
eN_e^{(1)}\left(\mathbf{E}^{(0)}+\frac{1}{c}\mathbf{U}_e^{(0)}\times\mathbf{B}^{(0)}\right)+\\
eN_i^{(0)}\left(\mathbf{E}^{(1)}+\frac{1}{c}\mathbf{U}_e^{(1)}\times\mathbf{B}^{(0)}+\frac{1}{c}\mathbf{U}_e^{(0)}\times\mathbf{B}^{(1)}\right)+\nabla p_e^{(1)}-\\
m_e N_e \upsilon_{ei}\left(\mathbf{U}_i^{(0)}-\mathbf{U}_e^{(0)}\right)=0.
\end{gathered}
\tag{6.9}
$$

Define the first order current density as

$$
\mathbf{J}^{(1)}=\sum_a e_a\left(N_a^{(0)}\mathbf{U}_a^{(1)}+N_a^{(1)}\mathbf{U}_a^{(0)}\right). \tag{6.10}
$$

and assume low β, so that $B^{(1)}$=0 and $\partial B^{(0)}/\partial t$=0. The superscript (0) on $B^{(0)}$ will be dropped from now on. Taking the scalar product of B with the electron and ion equations, taking a flux surface average, and summing the results leads to the parallel momentum equation:

$$
m_i N_i \frac{\partial}{\partial t} < \mathbf{B}\cdot\mathbf{U} > = - < \mathbf{B}\cdot\nabla\cdot\mathbf{D} > - m_i N_i < \upsilon_{in}\mathbf{B}\cdot\mathbf{U} > . \tag{6.11}
$$

Note that the superscript (0) has been dropped from the densities and flows, as they are all 0^{th} order quantities. The same process can be applied using the poloidal magnetic field to derive the poloidal momentum balance:

$$
m_i N_i \frac{\partial}{\partial t} < \mathbf{B}_P\cdot\mathbf{U} > = -\frac{\sqrt{g}B^{\zeta}B^{\alpha}}{c} < \mathbf{J}\cdot\nabla\rho > - < \mathbf{B}_P\cdot\nabla\cdot\mathbf{D} > - m_i N_i < \upsilon_{in}\mathbf{B}_P\cdot\mathbf{U} > . \tag{6.12}
$$

The ion-neutral collision frequency is given by $\nu_{in}=n_n<\sigma v>$, where $<\sigma v>$ is a rate coefficient defined such that the ion-neutral friction term in equation (6.12) works properly. The proper calculation of this rate coefficient is discussed in Appendix 3. Unlike the ion and electron density, the neutral density is not a flux surface constant. Hence, in the theoretical development here, we will write the neutral density as:

$$
n_n = n_{no} f_n(\alpha,\zeta). \tag{6.13}
$$

The inclusion of toroidally asymmetric neutrals is a new development in this dissertation, and the determination of $f_n(\alpha,\zeta)$ will be discussed in Section 6.3. Defining $\nu_{in0}=n_{no}<\sigma v>$, we can write the fluid equations as

$$m_i N_i \frac{\partial}{\partial t} < \mathbf{B} \cdot \mathbf{U} >= - < \mathbf{B} \cdot \nabla \cdot \mathbf{D} > - m_i N_i \upsilon_{in0} < f_n(\alpha, \zeta) \mathbf{B} \cdot \mathbf{U} >, \tag{6.14}$$

$$\begin{aligned} m_i N_i \frac{\partial}{\partial t} < \mathbf{B}_P \cdot \mathbf{U} >= -\frac{\sqrt{g} B^\zeta B^\alpha}{c} < \mathbf{J} \cdot \nabla \rho > - < \mathbf{B}_P \cdot \nabla \cdot \mathbf{D} > \\ - m_i N_i \upsilon_{in0} < f_n(\alpha, \zeta) \mathbf{B}_P \cdot \mathbf{U} > . \end{aligned} \tag{6.15}$$

In these equations, it is necessary to specify a form for the viscosity. In the limits of low flow speed in the plateau or Pfirsch-Schlueter regime, the viscosities can be calculated as

$$\langle \mathbf{B} \cdot \nabla \cdot \mathbf{D} \rangle = \mu_\alpha U^\alpha + \mu_\varsigma U^\varsigma, \tag{6.16a}$$

$$\langle \mathbf{B}_P \cdot \nabla \cdot \mathbf{D} \rangle = \mu_\alpha^{(P)} U^\alpha + \mu_\varsigma^{(P)} U^\varsigma. \tag{6.16b}$$

The coefficients μ have been calculated for the Pfirsch-Schlueter regime[4] and the plateau regime.[5] This calculation will be discussed in more in Section 6.3. Ions in HSX are generally in the plateau regime, as demonstrated in Section 3.4.

Radial currents flowing in the plasma need to satisfy the radial component of Ampere's law, given by

$$-\frac{\partial}{\partial t} \frac{\partial \Phi}{\partial \rho} < \nabla \rho \cdot \nabla \rho >= -4\pi \left(< \mathbf{J}^{(1)} \cdot \nabla \rho > + < \mathbf{J}_{ext}^{(1)} \cdot \nabla \rho > \right). \tag{6.17}$$

In this expression, we have used the relationship $\mathbf{E}=-\nabla\Phi=-(\partial\Phi/\partial\rho)\nabla\rho$. This equation shows that in steady state, any externally driven radial current is balanced by a return current, so that the net current is zero.

In this development, it will be convenient to cast the fluid equations in terms of the force free parallel flows and potential gradients. In doing so, it is useful to define a set of viscous damping frequencies

$$\upsilon_\alpha = \frac{\mu_\alpha B^\zeta}{m_i N_i < B^2 >}, \tag{6.18a}$$

$$\upsilon_\zeta = \frac{\mu_\zeta B^\zeta}{m_i N_i < B^2 >}, \tag{6.18b}$$

$$\upsilon_\alpha^{(P)} = \frac{\mu_\alpha^{(P)} B^\alpha}{m_i N_i < B_P^2 >}, \tag{6.18c}$$

$$\upsilon_\zeta^{(P)} = \frac{\mu_\zeta^{(P)} B^\alpha}{m_i N_i < B_P^2 >}. \tag{6.18d}$$

The radial force balance equations can be solved in steady state to yield an estimate of the radial conductivity of the plasma. By using the (6.6), (6.7), (6.16) and (6.18) in the steady state parallel momentum balance, the constant λ can be written as

$$\lambda = -\frac{\overline{C}}{B^\zeta \sqrt{g}} \left(\frac{\mu_\alpha + m_i N_i \upsilon_{in0} \left\langle f_n(\alpha,\zeta) B_\alpha \right\rangle}{B \cdot \mu + m_i N_i \upsilon_{in0} \left\langle f_n(\alpha,\zeta) B^2 \right\rangle} \right). \tag{6.19}$$

where $B \cdot \mu = B^\alpha \mu_\alpha + B^\zeta \mu_\zeta$, and

$$\overline{C} = c \left(\frac{\partial \Phi}{\partial \rho} + \frac{1}{eN_i} \frac{\partial p_i}{\partial \rho} \right). \tag{6.20}$$

This expression for λ can be inserted into equations (6.6) and (6.7) to yield expressions for the contravariant toroidal and poloidal flow velocities:

$$U^\alpha = \frac{\overline{C}}{\sqrt{g}} \left(\frac{\mu_\zeta + m_i N_i \upsilon_{in0} \left\langle f_n(\alpha,\zeta) B_\zeta \right\rangle}{B \cdot \mu + m_i N_i \upsilon_{in0} \left\langle f_n(\alpha,\zeta) B^2 \right\rangle} \right), \tag{6.21}$$

$$U^\zeta = -\frac{\overline{C}}{\sqrt{g}} \left(\frac{\mu_\alpha + m_i N_i \upsilon_{in0} \left\langle f_n(\alpha,\zeta) B_\alpha \right\rangle}{B \cdot \mu + m_i N_i \upsilon_{in0} \left\langle f_n(\alpha,\zeta) B^2 \right\rangle} \right). \tag{6.22}$$

When $\mathbf{U} = U^\zeta \mathbf{e}_\zeta + U^\alpha \mathbf{e}_\alpha$ and the linear poloidal viscosity are inserted in the poloidal momentum balance, the flows can be related to the radial current as

$$\left\langle \bar{J} \cdot \nabla \rho \right\rangle = -\frac{c m_i N_i \left\langle \mathbf{B}_P \cdot \mathbf{B}_P \right\rangle}{\sqrt{g} B^\alpha B^\alpha B^\zeta} \left(\begin{array}{l} \left[\upsilon_\alpha^{(P)} + \upsilon_{in0} \dfrac{\left\langle f_n(\alpha,\zeta) \mathbf{B}_P \cdot \mathbf{B}_P \right\rangle}{\left\langle \mathbf{B}_P \cdot \mathbf{B}_P \right\rangle} \right] U^\alpha + \\ \left[\upsilon_\zeta^{(P)} + \iota \upsilon_{in0} \dfrac{\left\langle f_n(\alpha,\zeta) \mathbf{B}_P \cdot \mathbf{B}_T \right\rangle}{\left\langle \mathbf{B}_P \cdot \mathbf{B}_P \right\rangle} \right] U^\zeta \end{array} \right). \tag{6.23}$$

Finally, the expressions relating flows to the electric field, (6.21) and (6.22), can be inserted in (6.23) to yield the radial current in terms of the electric field as:

$$\left\langle \mathbf{J}\cdot\nabla\psi \right\rangle = \sigma_\perp \left(-\left\langle \mathbf{E}_r \cdot \nabla\psi \right\rangle + \frac{\left\langle \nabla p_i \cdot \nabla\psi \right\rangle}{eN_i} \right). \tag{6.24}$$

In deriving this expression, the relationship

$$\mathbf{E}_r = -\frac{\partial\Phi}{\partial\psi}\nabla\psi \tag{6.25}$$

was used, and the radial conductivity $\sigma_\perp$ is defined as

$$\sigma_\perp = -\frac{c^2 m_i N_i \left\langle B_P^2 \right\rangle}{\left\langle \nabla\psi\cdot\nabla\psi \right\rangle \left(\sqrt{g} B^\alpha B^\zeta\right)^2 \left(\iota\upsilon_\alpha + \upsilon_\zeta + \upsilon_{in} \dfrac{\left\langle f_n(\alpha,\zeta) B^2 \right\rangle}{\left\langle B^2 \right\rangle} \right)} \times$$
$$\left[\left(\upsilon_\alpha^{(P)} + \upsilon_{in0} \frac{\left\langle f_n(\alpha,\zeta) \mathbf{B}_P \cdot \mathbf{B}_P \right\rangle}{\left\langle B_P^2 \right\rangle} \right) \left(\upsilon_\zeta + \upsilon_{in0} \frac{\left\langle f_n(\alpha,\zeta) \mathbf{B}\cdot\mathbf{B}_T \right\rangle}{\left\langle B^2 \right\rangle} \right) - \left(\upsilon_\zeta^{(P)} + \iota\upsilon_{in0} \frac{\left\langle f_n(\alpha,\zeta) \mathbf{B}_P \cdot \mathbf{B}_T \right\rangle}{\left\langle B_P^2 \right\rangle} \right) \left(\upsilon_\alpha + \upsilon_{in0} \frac{\left\langle f_n(\alpha,\zeta) \mathbf{B}\cdot\mathbf{B}_P \right\rangle}{\iota\left\langle B^2 \right\rangle} \right) \right]. \tag{6.26}$$

Note that when the external current $<\mathbf{J}\cdot\nabla\psi>$ is zero, (6.24) implies that the electric field is exactly balanced by the pressure gradient. There are both **E**x**B** and diamagnetic flows, which exactly cancel each other. This then implies from (6.21) and (6.22) that no net plasma flow is present in the absence of a radial current. Recall that the ion temperature gradient is not included in the modeling. If terms in the viscosity proportional to the heat flux had been kept in the modeling, then flow at zero radial current would occur.

In anticipation of a comparison between hydrogen and deuterium discharges, it is interesting to see how the neoclassical radial conductivity scales with the mass of the ion species. In the limit that a toroidally and poloidally uniform ion-neutral frequency dominates all of the viscous frequencies, the expression for the radial conductivity reduces to

$$\sigma_{\perp} = -\frac{c^2 m_i N_i \left\langle B_P^2 \right\rangle}{\left\langle \nabla\psi \cdot \nabla\psi \right\rangle \left(\sqrt{g} B^{\alpha} B^{\zeta}\right)^2} \upsilon_{in} \tag{6.27}$$

In this limit, the radial conductivity scales linearly with the ion mass. This expression shows scaling similar to the classical Yoshikawa radial conductivity.[6]

On the other hand, if the viscous frequency terms in (6.26) dominate all of the neutral friction terms, than the radial conductivity reduces to an expression

$$\sigma_{\perp} = -\frac{\kappa}{\left\langle \nabla\psi \cdot \nabla\psi \right\rangle} \left(\frac{2\pi c}{\iota}\right)^2 \frac{\alpha_P \left(B^{\zeta}\alpha_T + B^{\alpha}\alpha_C\right) - \alpha_C \left(B^{\alpha}\alpha_P + B^{\zeta}\alpha_C\right)}{\iota \left(B^{\alpha}\alpha_P + B^{\zeta}\alpha_C\right) + \left(B^{\zeta}\alpha_T + B^{\alpha}\alpha_C\right)} \tag{6.28}$$

This expression has assumed the results of Section 6.2, where the viscosity coefficients are calculated. It suffices for now to note that α_T, α_C, and α_P are purely geometric factors related to the magnetic field spectrum. For the plateau regime, the factor κ is given by $\kappa=\pi^{1/2}PB_o/v_{ta}B^{\zeta}$. Hence, for all other parameters fixed in a plateau regime plasma with vanishingly small neutral density, the radial conductivity should scale like $m_i^{1/2}$. In the Pfirsch-Schlueter regime, $\kappa=\mu_o P/\nu_{ii}$. Hence, the radial conductivity should also scale like $m_i^{1/2}$ in this case.

There is a regime intermediate to these two limits, where the ion-neutral collision frequency dominates some, but not all, of the viscous frequencies. An example of this situation is an axisymmetric tokamak with neutrals, where the toroidal damping is dominated by neutrals but the poloidal damping is determined by the poloidal viscosity. It has been shown[7] that in the plateau regime in this configuration, the combination of poloidal viscosity and neutral friction can cause a significant increase in the neoclassical radial conductivity compared to the Yoshikawa conductivity. In this case, the scaling of the radial conductivity with ion mass is not perfectly clear; it depends on the interplay between a number of terms and no generic answer is possible. The equivalent calculation for HSX would be to include only the (n,m)=(4,1) component of the magnetic field and ion-neutral friction. Unfortunately, no small and simple formula can be written for the radial conductivity in this case; the mass scaling of the radial conductivity has to be calculated for the appropriate plasma parameters. These calculations will be presented in Section 7.1.4.

With expression (6.24) relating the radial current and the electric field, expressions (6.21) and (6.22) can be used to solve for the direction of the flow. The result is

$$U^{\zeta} = -KB^{\zeta}\left(\iota\upsilon_{\alpha} + \upsilon_{in0}\frac{\langle f_n(\alpha,\zeta)\mathbf{B}\cdot\mathbf{B}_P\rangle}{\langle B^2\rangle}\right), \tag{6.29}$$

$$U^{\alpha} = KB^{\alpha}\left(\upsilon_{\zeta} + \upsilon_{in0}\frac{\langle f_n(\alpha,\zeta)\mathbf{B}\cdot\mathbf{B}_T\rangle}{\langle B^2\rangle}\right). \tag{6.30}$$

In these expressions, the constant K is related to the radial current as

$$K = \frac{c\langle \mathbf{J}\cdot\nabla\rho\rangle}{\left(\sqrt{g}B^{\alpha}B^{\zeta}\right)\langle\nabla\psi\cdot\nabla\psi\rangle\sigma_{\perp}\left(\iota\upsilon_{\alpha} + \upsilon_{\zeta} + \upsilon_{in0}\frac{\langle f_n(\alpha,\zeta)B^2\rangle}{\langle B^2\rangle}\right)}. \tag{6.31}$$

6.2 Evaluation of the Viscosities in the Plateau and Pfirsch-Schlueter Regimes.

Before solving the fluid equations for the time evolution of the flow, it is necessary to calculate the viscosity coefficients in equation (6.16). The magnetic field in Hamada coordinates can be written as

$$B = B_o\left(1 + \sum_{n,m\neq 0} B_{nm}(\alpha,\zeta)\right) = B_o\left(1 + \sum_{n,m\neq 0}\varepsilon_{nm}\,\mathbf{cos}(m\alpha - n\zeta)\right). \tag{6.32}$$

In the case of the plateau regime, the viscosities are given by[5]

$$\langle \mathbf{B}\cdot\nabla\cdot\mathbf{D}\rangle = 3\left(\mu^{P}_{a1}U^{\alpha} + \mu^{T}_{a1}U^{\zeta} + \frac{2}{5}\mu^{P}_{a2}\frac{q^{\alpha}}{p} + \frac{2}{5}\mu^{T}_{a2}\frac{q^{\zeta}}{p}\right), \tag{6.33a}$$

$$\langle \mathbf{B}_P\cdot\nabla\cdot\mathbf{D}\rangle = 3\left(\mu^{P}_{Pa1}U^{\alpha} + \mu^{T}_{Pa1}U^{\zeta} + \frac{2}{5}\mu^{P}_{Pa2}\frac{q^{\alpha}}{p} + \frac{2}{5}\mu^{T}_{Pa2}\frac{q^{\zeta}}{p}\right), \tag{6.33b}$$

where, for j=1-2,

$$\mu_{aj}^{P} = \frac{\sqrt{\pi}}{3} P_a C_j \sum_{m,n\neq 0} \left\langle \frac{\mathbf{B}\cdot\nabla B}{B} \frac{\partial B_{nm}}{\partial \alpha} \right\rangle \left(\omega_{ta}^{nm}\right)^{-1}, \tag{6.34a}$$

$$\mu_{aj}^{T} = \frac{\sqrt{\pi}}{3} P_a C_j \sum_{m,n\neq 0} \left\langle \frac{\mathbf{B}\cdot\nabla B}{B} \frac{\partial B_{nm}}{\partial \zeta} \right\rangle \left(\omega_{ta}^{nm}\right)^{-1}, \tag{6.34b}$$

$$\mu_{Paj}^{P} = \frac{\sqrt{\pi}}{3} P_a C_j \sum_{m,n\neq 0} \left\langle \frac{\mathbf{B}_P\cdot\nabla B}{B} \frac{\partial B_{nm}}{\partial \alpha} \right\rangle \left(\omega_{ta}^{nm}\right)^{-1}, \tag{6.34c}$$

$$\mu_{Paj}^{T} = \frac{\sqrt{\pi}}{3} P_a C_j \sum_{m,n\neq 0} \left\langle \frac{\mathbf{B}_P\cdot\nabla B}{B} \frac{\partial B_{nm}}{\partial \zeta} \right\rangle \left(\omega_{ta}^{nm}\right)^{-1}, \tag{6.34d}$$

and $C_1=\Gamma(3)$, $C_2=\Gamma(4)-5\Gamma(3)/2$. P_a is the pressure of the species under consideration, and

$$\left(\omega_{ta}^{nm}\right)^{-1} = v_{ta} \left| mB^{\alpha} - nB^{\zeta} \right| / B_o . \tag{6.35}$$

In calculations to date, the heat flux has been ignored, which is tantamount to setting the ion temperature gradient to zero. As noted above, the inclusion of this term would lead to rotation proportional to the ion temperature gradient. This would require solving the heat flux balance equation as well as the momentum and continuity equations,[8] and is beyond the scope of this work.

By ignoring the heat flux, the expressions for the viscosity can be simplified considerably to a general result of the form

$$\left\langle \mathbf{A}\cdot\nabla\cdot\mathbf{D} \right\rangle = \frac{2\sqrt{\pi} P_a B_o}{v_{ta} B^{\zeta}} \sum_{n,m\neq 0} \frac{1}{\left| n - m\iota \right|} \left\langle \frac{\mathbf{A}\cdot\nabla\mathbf{B}}{B} \mathbf{U}\cdot\nabla B_{nm} \right\rangle, \tag{6.36}$$

with $\mathbf{A}=\mathbf{B}_T$, $\mathbf{B}_P$, or $\mathbf{B}$. To evaluate this expression, first note that the term in the flux surface average can be written as

$$\left\langle \frac{\mathbf{A}\cdot\nabla B}{B}\mathbf{U}\cdot\nabla B_{nm}\right\rangle = B_o\left(\begin{array}{l} A^{\zeta}U^{\zeta}\left\langle\frac{S_1S_3}{B}\right\rangle - A^{\zeta}U^{\alpha}\left\langle\frac{S_1S_4}{B}\right\rangle \\ -A^{\alpha}U^{\zeta}\left\langle\frac{S_2S_3}{B}\right\rangle + A^{\alpha}U^{\alpha}\left\langle\frac{S_2S_4}{B}\right\rangle \end{array}\right), \tag{6.37}$$

where

$$S_1 = \sum_{n,m\neq 0} n\varepsilon_{nm}\,\mathbf{sin}(m\alpha - n\zeta), \tag{6.38a}$$

$$S_2 = \sum m\varepsilon_{nm}\,\mathbf{sin}(m\alpha - n\zeta), \tag{6.38b}$$

$$S_3 = n'\varepsilon_{n'm'}\,\mathbf{sin}(m'\alpha - n'\zeta), \tag{6.38c}$$

$$S_4 = m'\varepsilon_{n'm'}\,\mathbf{sin}(m'\alpha - n'\zeta). \tag{6.38d}$$

The next step is to evaluate the flux surface averages in the expression above. As an example, the quantity $<S_1S_3/B>$ will be evaluated below. This quantity can be written as

$$\left\langle\frac{S_1S_3}{B}\right\rangle = \left\langle \frac{\sum_{n,m\neq 0} n\varepsilon_{nm}\sin(m\alpha - n\zeta)n'\varepsilon_{n'm'}\sin(m'\alpha - n'\zeta)}{B_o\left(1+\sum_{n'',m''\neq 0}\varepsilon_{n''m''}\cos(m''\alpha - n''\zeta)\right)}\right\rangle. \tag{6.39}$$

For $\varepsilon_{n,m}$<<1, the sum in the denominator can be neglected. Utilizing the definition of the flux surface average the yields

$$\left\langle\frac{S_1S_3}{B}\right\rangle = \frac{1}{4\pi^2B_o}\int_0^{2\pi}\int_0^{2\pi}\sum_{n,m\neq 0} n\varepsilon_{nm}\,\mathbf{sin}(m\alpha - n\zeta)n'\varepsilon_{n'm'}\,\mathbf{sin}(m'\alpha - n'\zeta)d\zeta d\alpha\,. \tag{6.40}$$

The orthogonality relationship between sines,

$$\int_0^{2\pi}\int_0^{2\pi}\mathbf{sin}(m\alpha - n\zeta)\mathbf{sin}(m'\alpha - n'\zeta) = \begin{cases}2\pi^2 \\ 0\end{cases}, \tag{6.41}$$

allows the flux surface average to be evaluated as

$$\left\langle \frac{S_1 S_3}{B} \right\rangle = \frac{n^2 \varepsilon_{nm}^2}{2B_o}. \tag{6.42}$$

Using this expression and the other similar flux surface averages, it is then easy to show that

$$\langle \mathbf{A} \cdot \nabla \cdot \mathbf{D} \rangle = \kappa \left[U^\xi \left(A^\xi \alpha_T + A^\alpha \alpha_C \right) + U^\alpha \left(A^\alpha \alpha_P + A^\xi \alpha_C \right) \right]. \tag{6.43}$$

In this expression, the constants are defined as

$$\alpha_T = \sum_{n,m \neq 0} \frac{n^2 \varepsilon_{nm}^2}{|n - m\iota|}, \tag{6.44a}$$

$$\alpha_C = -\sum_{n,m \neq 0} \frac{nm \varepsilon_{nm}^2}{|n - m\iota|}, \tag{6.44b}$$

$$\alpha_P = \sum_{n,m \neq 0} \frac{m^2 \varepsilon_{nm}^2}{|n - m\iota|}, \tag{6.44c}$$

$$\kappa = \frac{\sqrt{\pi} P_a B_o}{v_{ta} B^\xi}. \tag{6.45}$$

As expected for the plateau regime, these expressions are independent of the collision frequency. With these definitions, the plateau linear viscosity is fully defined.

The viscosity for the Pfirsch-Schlueter regime has been specified as[4]

$$\langle \mathbf{A} \cdot \nabla \cdot \mathbf{D} \rangle = \frac{\mu_o P_a}{\upsilon_{ii}} \left\langle \frac{\mathbf{A} \cdot \nabla B}{B} \frac{\mathbf{U}_a \cdot \nabla B}{B} \right\rangle, \tag{6.46}$$

where μ_o=4.095 and ν_{ii} is the ion collision frequency. This expression can be evaluated using techniques similar to those above. The final result will be the same as above but with certain coefficients redefined:

$$\alpha_T = \sum_{n,m \neq 0} \frac{n^2 \varepsilon_{nm}^2}{2}, \tag{6.47a}$$

$$\alpha_C = -\sum_{n,m \neq 0} \frac{nm \varepsilon_{nm}^2}{2}, \tag{6.47b}$$

$$\alpha_P = \sum_{n,m\neq 0} \frac{m^2 \varepsilon_{nm}^2}{2}, \tag{6.47c}$$

$$\kappa = \frac{\mu_o P_a}{\upsilon_{ii}}. \tag{6.48}$$

Finally, the viscosity coefficients needed in the momentum equation can be derived from these expressions as

$$\mu_\alpha = \kappa\left(B^\alpha \alpha_P + B^\zeta \alpha_C\right), \tag{6.49a}$$

$$\mu_\zeta = \kappa\left(B^\zeta \alpha_T + B^\alpha \alpha_C\right), \tag{6.49b}$$

$$\mu_\alpha^{(P)} = \kappa B^\alpha \alpha_P, \tag{6.49c}$$

$$\mu_\zeta^{(P)} = \kappa B^\alpha \alpha_C, \tag{6.49d}$$

6.3 Determination of the Neutral Weighting Function.

The function $f_n(\alpha,\zeta)$ is determined by a combination of atomic physics and the way that HSX is fueled. For discharges described in this work, gas was allowed into the torus using a puff valve with a waveform preprogrammed to maintain a flat density throughout the discharge. This is a toroidally and poloidally localized source. In addition, there is some recycling from the wall, leading to a more spatially uniform source.

The rate coefficients for proton and electron impact ionization of a hydrogen atom are shown in figure 6.1, where data has been collected from a number of sources as a check on consistency.[9,10,11,12] Note that for HSX relevant ion temperatures ($\approx$25 eV), proton impact ionization is irrelevant.

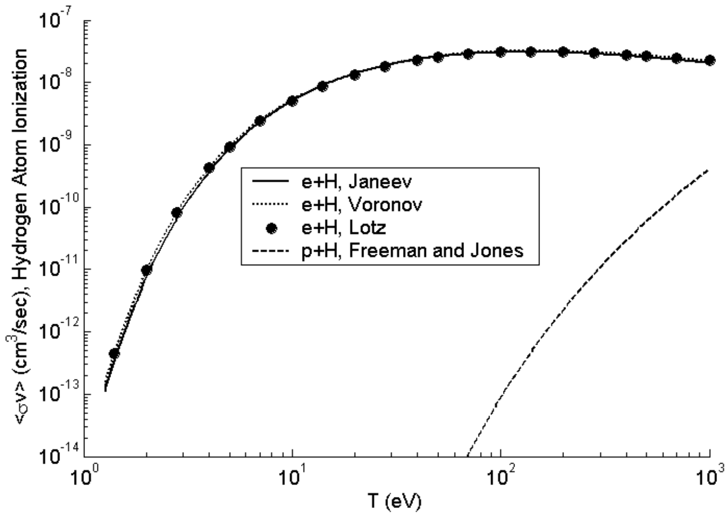

Figure 6.1 Rate coefficient for hydrogen atom ionization.

For HSX electron temperatures of a few hundred electron volts, the rate coefficient for electron impact ionization is flat with a value of $\approx 2.5\times10^{-8}$ cm^3s^{-1}, as illustrated in figure 6.1. For an electron density of $1\text{x}10^{12}$ cm^{-3}, the mean free path for a Frank-Condon ($\approx$3eV) neutral is

$$\lambda_{mfp,H} = \frac{\sqrt{\frac{2\cdot 3\cdot 1.6\times10^{-19}}{1.67\times10^{-27}}}\left(\frac{m}{s}\right)}{2.5\times10^{-8}\left(cm^3s^{-1}\right)\cdot 10^{12}cm^{-3}} \approx 1m. \tag{6.50}$$

This is significantly larger than the minor radius of the plasma ($\approx$10 to 15 cm), but smaller than the circumference (circumference=πD$\approx$7.5 meters). Hence, it is expected that there should be very little variation in the atomic hydrogen density at any fixed toroidal angle, but there can be a large toroidal asymmetry due to the localized gas puff.

The rate coefficients for processes which eliminate hydrogen molecules are shown in figure 6.2, using the data presented by Janeev. Processes which eliminate molecules include electron impact dissociation, electron impact ionization, and proton impact ionization. Electron impact ionization dominates electron impact dissociation for HSX temperatures, and proton impact ionization can be ignored.

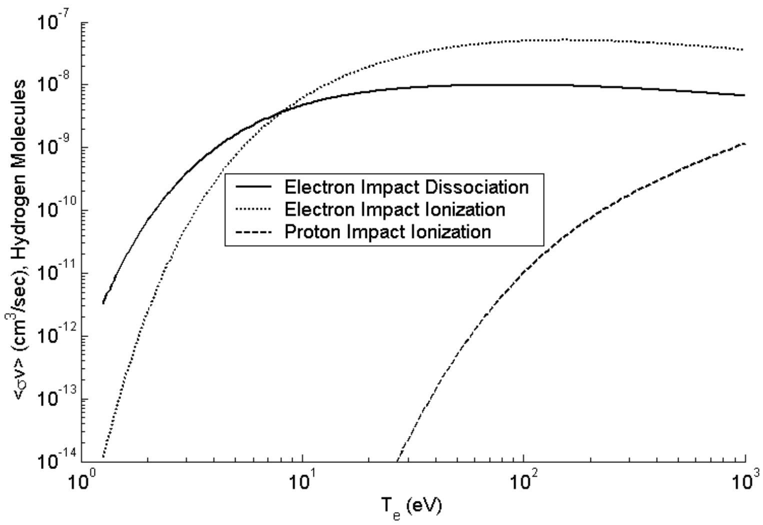

Figure 6.2 Rate coefficient for hydrogen molecule ionization.

The effective mean free path for molecules in HSX can be calculated as above, with the assumption that the molecules are at room temperature:

$$\lambda_{mfp,H_2} = \frac{\sqrt{\frac{2\cdot .025\cdot 1.6\times 10^{-19}}{1.67\times 10^{-27}}}\left(\frac{m}{s}\right)}{4.5\times 10^{-8}\left(cm^3 s^{-1}\right)\cdot 10^{12}\,cm^{-3}} \approx 5cm\,. \tag{6.51}$$

This length is much smaller than the mean free path of atoms, mainly due to the reduced velocity of the molecules compared to the atoms. Hence, we can assume that the concentration of hydrogen molecules will vary toroidally as well as radially at a given cross section.

Data from the H_α arrays have been used in conjunction with the interferometer data as input to the DEGAS[13] code. There calculations were done by John Canik, and only the results will be described here. This combination of measurements and modeling allows the calculation of the toroidal variation of the neutral atoms and molecules in HSX. The average neutral density at each toroidal angle has been plotted versus toroidal angle in figure 6.3. The data points in these curves correspond to the average neutral density in the plane at fixed toroidal angle. The gas puff is located at 200°. The left plot shows that the concentration of hydrogen molecules is everywhere greater than hydrogen atoms, and that both species have a peak at the gas puffer. The ratio of molecular to atomic density is shown on the right, where the reduction in the ratio on either side of the puffer is due to the longer mean free path of atoms compared to molecules.

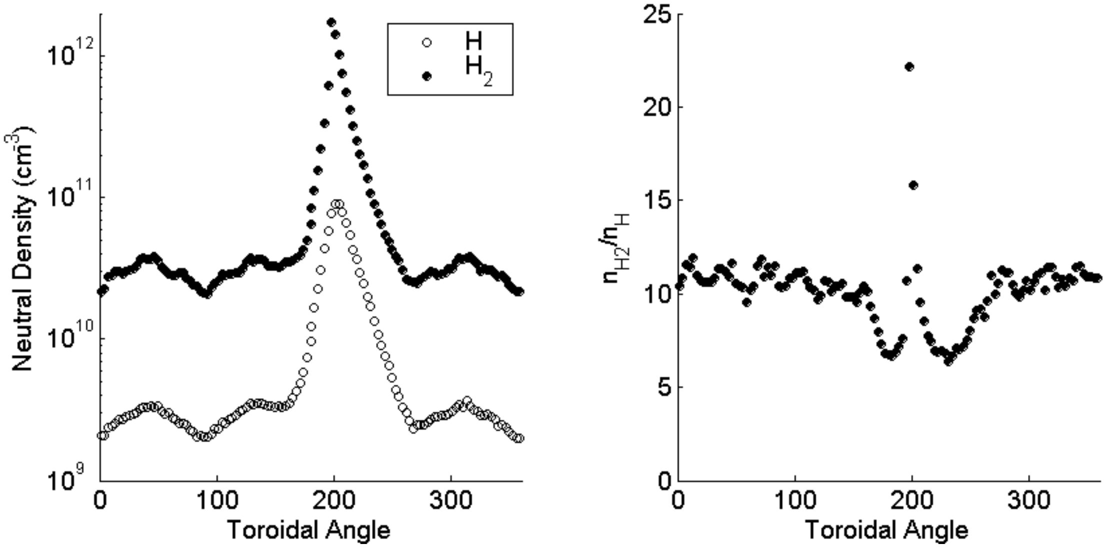

Figure 6.3: Toroidal distribution of atomic and molecular hydrogen (left) and ratio of molecular to atomic hydrogen (right). DEGAS calculations were performed by John Canik.

A detailed discussion of the processes by which ion-neutral interactions damp flows is presented in Appendix 3. It is shown there that both elastic scattering and charge exchange cause damping of plasma flows due to interactions with neutrals. Further, collisions of protons with both hydrogen molecules and atoms must be considered. The effective rate coefficients for these processes are shown in figure 6.4. The curve on the left for p+H collisions is dominated by charge exchange. For the p+H_2 collisions, the peak at low ion temperature is due to elastic scattering, while the rise toward higher ion temperature is due to charge exchange. The ratio of these curves is shown on the right. At HSX relevant ion temperatures of 20-30 eV, the effective rate coefficient for p+H collisions is more than 100 times greater than the rate coefficient for p+H_2 collisions. Looking back at figure 6.3, the molecular hydrogen density exceeds the atomic density by at most a factor of 25, and this in only a very small region. Hence, ion neutral friction on molecular hydrogen will be ignored in the modeling.

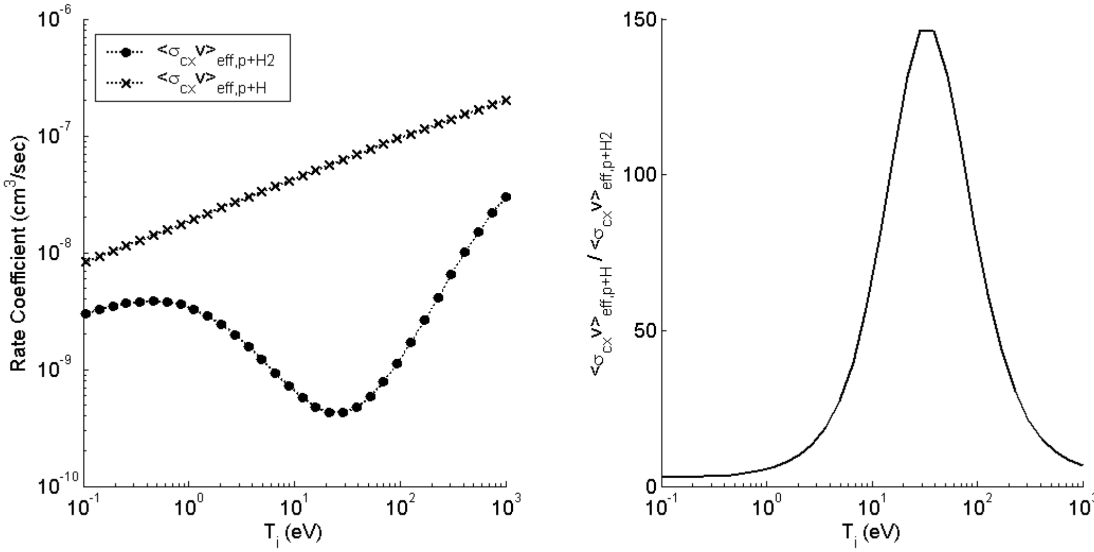

Figure 6.4: Effective rate coefficients for momentum scattering from p+H (×) and p+H_2 (•) collisions (left), and the ratio of the rate coefficients (right).

With this information, it is possible to specify the function $f_n(\alpha,\zeta)$. The Hamada toroidal angle (ζ) and the lab toroidal angle (φ) are nearly identical, so they are used interchangeably. The toroidal distribution of the hydrogen atoms is fit to a function of the form

$$n_n(\zeta) = n_{n0}\left(1 + \sum_k A_k \,\mathbf{exp}\left(-\frac{(\zeta - C_k)^2}{W_k^2}\right)\right). \tag{6.52}$$

In this expression, C_k is the toroidal angle of the source, and W_k represents the toroidal extend of the neutral gas distribution. Here k is an index over the number of discrete sources, and is usually restricted to k=1. An example of this fit is shown in figure 6.5. The resulting fit curve is used when calculating the flux surface averages, as described in Chapter 5. Note that with this fitting function, n_{n0} represents the density in the wings of the function far from the source, not the average atomic hydrogen density around the machine.

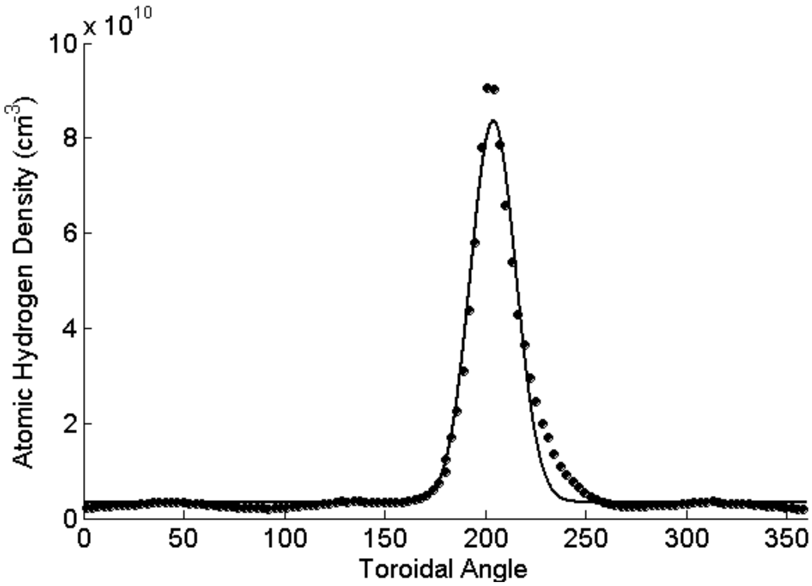

Figure 6.5: Fit to toroidal variation of atomic hydrogen.

6.4 Different Time Dependent Solutions to the Fluid Equation.

This section will describe in detail the solution of the fluid equations for the time evolution of the plasma flows. Section 6.4.1 will cast the fluid equations in a form that will be useful for calculation. Section 6.4.2 will review the Coronado and Talmadge formulation of the problem. This solution is used to study the flow and electric field relaxation when the electrode current is terminated. An original model for the flow spin-up will be discussed in Section 6.4.3. Comparisons between the two models and their synthesis will be presented in 6.4.4.

6.4.1: Simplification of the Fluid Equations.

To solve the time dependent problem, the fluid equations are written in terms of the bootstrap flow (λ) and the electric field ($d\Phi/d\rho$). The poloidal momentum balance equation becomes

$$a_1 \frac{\partial}{\partial t}\frac{\partial \Phi}{\partial \rho} + a_2 \frac{\partial \lambda_i}{\partial t} + b_1 \frac{\partial \Phi}{\partial \rho} + b_2 \lambda_i = C_1. \tag{6.53}$$

where of the constants are defined as

$$a_1 = \left(1 + \frac{\left(\sqrt{g}B^{\alpha}B^{\varsigma}\right)^2 < \nabla\rho \cdot \nabla\rho >}{4\pi c^2 m_i N_i \left\langle B_p^2 \right\rangle}\right), \tag{6.54a}$$

$$a_2 = \frac{\sqrt{g}B^{\alpha}B^{\varsigma}}{c} \frac{\left\langle \mathbf{B} \cdot \mathbf{B}_p \right\rangle}{\left\langle \mathbf{B}_p \cdot \mathbf{B}_p \right\rangle}, \tag{6.54b}$$

$$b_1 = \upsilon_{\alpha}^{(P)} + \upsilon_{in0} \frac{\left\langle f_n(\alpha,\zeta)\mathbf{B}_P \cdot \mathbf{B}_p \right\rangle}{\left\langle \mathbf{B}_P \cdot \mathbf{B}_p \right\rangle}, \tag{6.54c}$$

$$b_2 = \frac{\sqrt{g}B^{\alpha}B^{\varsigma}}{c}\left(\upsilon_{\alpha}^{(P)} + q\upsilon_{\varsigma}^{(P)} + \upsilon_{in0} \frac{\left\langle f_n(\alpha,\zeta)\mathbf{B} \cdot \mathbf{B}_p \right\rangle}{\left\langle \mathbf{B}_p \cdot \mathbf{B}_p \right\rangle}\right), \tag{6.54d}$$

$$C_1 = \frac{\left(\sqrt{g}B^{\alpha}B^{\varsigma}\right)^2}{c^2 m_i N_i \left\langle \mathbf{B}_p \cdot \mathbf{B}_p \right\rangle}\left\langle \mathbf{J}_{ext} \cdot \nabla\rho \right\rangle - \left(\upsilon_{\alpha}^{(P)} + \upsilon_{in0} \frac{\left\langle f_n(\alpha,\zeta)\mathbf{B}_P \cdot \mathbf{B}_p \right\rangle}{\left\langle \mathbf{B}_p \cdot \mathbf{B}_p \right\rangle}\right)\frac{1}{eN_i}\frac{\partial p_i}{\partial \rho}, \tag{6.54e}$$

The parallel momentum balance equation can be similarly written as

$$a_3 \frac{\partial}{\partial t}\frac{\partial \Phi}{\partial \rho} + a_4 \frac{\partial \lambda_i}{\partial t} + b_3 \frac{\partial \Phi}{\partial \rho} + b_4 \lambda_i = C_2. \tag{6.55}$$

where the constants are written as

$$a_3 = \frac{\left\langle \mathbf{B} \cdot \mathbf{B}_p \right\rangle}{\left\langle B^2 \right\rangle}, \tag{6.56a}$$

$$a_4 = \frac{\sqrt{g}B^{\alpha}B^{\varsigma}}{c}, \tag{6.56b}$$

$$b_3 = \left(\mathfrak{t}\upsilon_{\alpha} + \upsilon_{in0} \frac{\left\langle f_n(\alpha,\zeta)\mathbf{B}_P \cdot \mathbf{B} \right\rangle}{\left\langle B^2 \right\rangle}\right), \tag{6.56c}$$

$$b_4 = \frac{\sqrt{g}B^{\alpha}B^{\varsigma}}{c}\left(\iota\upsilon_{\alpha} + \upsilon_{\zeta} + \upsilon_{in0}\frac{\langle f_n(\alpha,\zeta)\mathbf{B}\cdot\mathbf{B}\rangle}{\langle B^2\rangle}\right), \tag{6.56d}$$

$$C_2 = -\left(\iota\upsilon_{\alpha} + \upsilon_{in0}\frac{\langle f_n(\alpha,\zeta)\mathbf{B}_P\cdot\mathbf{B}\rangle}{\langle B^2\rangle}\right)\frac{1}{eN_i}\frac{\partial p_i}{\partial\rho}. \tag{6.56e}$$

In these expressions, a_1 and a_3 are dimensionless, while a_2 and a_4 have dimensions of statVolt·sec/cm^3. The dimensions of b_1 and b_3 are 1/sec, while b_2 and b_4 have units of statVolt/cm^3.

Before solving these equations for the flow and electric field evolution, it is instructive to recall a few points from the data presented in Chapter 4. Recall that the floating potential was observed to change very quickly when the electrode was energized, but to decay more slowly when the power supply was turned off. This asymmetry in the potential evolution leads to different methods in modeling the evolution of the plasma flow at the beginning or the end of the bias pulse.

At the bias turn-on, the first event is the solid state switches in the power supply going into conducting state and applying the capacitor bank voltage to the face of the electrode. In the data, we observe the floating potential rising on a very fast time scale, and a large spike in the electrode current. Given these observations, it appears that the most appropriate model for the spin-up of the plasma involves the electric field being defined as the initiating event, with the current and flows reacting to that drive.

At the electrode turn off, the first event is the solid state switches in the power supply breaking the electrode current, which is observed to occur in a ~1-2 μsec. The floating potential and plasma flows decay on longer time scale. Hence, the proper modeling of the spin-down appears to involve the electrode current termination as the initiating event.

6.4.2: Coronado and Talmadge Model.

In the Coronado and Talmadge model, the evolution of the external radial current is specified as an arbitrary function of time. The coupled fluid equations are solved to find the evolution of the force free flow and the potential gradient. This is done in detail in their paper, and a more general discussion of the differential equation solution method can be found in books on differential equations.[14]

To begin with, the fluid equations (6.53) and (6.55) are written in matrix form as

$$A\frac{d\mathbf{X}}{dt} + B\mathbf{X} = C. \tag{6.57}$$

In this expression, X=[$\partial\Phi/\partial\rho$; λ], and A, B, and C contain the constants in (6.54) and (6.56) above. The determinant of the matrix A is defined by

$$\Delta = \mathbf{det}(A) = a_4 a_1 - a_2 a_3. \tag{6.58}$$

Note that Δ has units of statVolt·sec/cm^3. Assuming that Δ is not zero, the matrix A can be inverted to yield the system of equations

$$\frac{d\mathbf{X}}{dt} = D\mathbf{X} + S \tag{6.59}$$

with D=A^{-1}B and S=A^{-1}C. From these expressions, it is possible to derive expressions for two damping rates, the eigenvalues of the system. These are given by

$$\left.\begin{matrix}\gamma_1\\ \gamma_2\end{matrix}\right\} = \frac{1}{2}(d_{11} + d_{22}) \pm \sqrt{\frac{1}{4}(d_{11} + d_{22})^2 - (d_{11}d_{22} - d_{12}d_{21})}. \tag{6.60}$$

These two damping rates are completely determined by the ion-neutral collision frequency and the magnetic geometry of the configuration. They are typically less than zero, corresponding to damping of the flow. The rate with larger absolute value is called the “fast rate” and the rate with smaller absolute value is called the “slow rate”.

Consider first the case that the external current is turned on as a step function. Although this case is probably not strictly applicable to HSX, it is illustrative to work out the details. The full time evolution of the flows and electric field can be calculated analytically. A series of constants need to be defined as:

$$C_{10} = -\left(\upsilon_{\alpha}^{(P)} + \upsilon_{in}\right)\frac{1}{eN_i}\frac{\partial p_i}{\partial \rho}, \tag{6.61a}$$

$$\partial C_1 = \frac{\left(\sqrt{g}B^{\alpha}B^{\varsigma}\right)^2}{c^2 m_i N_i \left\langle B_p^2 \right\rangle}\left\langle \mathbf{J}_{ext}\cdot\nabla\rho \right\rangle, \tag{6.61b}$$

$$F_0 = \frac{1}{\gamma_2\gamma_1\Delta}\left[b_4 C_{10} - b_2 C_4\right] = \frac{-1}{eN_i}\frac{\partial p_i}{\partial \rho}, \tag{6.61c}$$

$$F_1 = -\frac{\partial C_1}{\left(\gamma_2 - \gamma_1\right)\gamma_1\Delta}\left[d_{12}a_3 + \left(\gamma_2 - d_{11}\right)a_4\right], \tag{6.61d}$$

$$F_2 = \frac{\partial C_1}{\left(\gamma_2 - \gamma_1\right)\gamma_2\Delta}\left[d_{12}a_3 + \left(\gamma_1 - d_{11}\right)a_4\right], \tag{6.61e}$$

$$G_1 = -\frac{\partial C_1}{\left(\gamma_2 - \gamma_1\right)\gamma_1\Delta}\left[\left(\gamma_1 - d_{11}\right)a_3 - d_{21}a_4\right], \tag{6.61f}$$

$$G_2 = \frac{\partial C_1}{\left(\gamma_2 - \gamma_1\right)\gamma_2\Delta}\left[\left(\gamma_2 - d_{11}\right)a_3 - d_{21}a_4\right]. \tag{6.61g}$$

The time evolution of all quantities will be specified through the two functions

$$T_1 = \left(1 - e^{\gamma_1 t}\right), \tag{6.62a}$$

$$T_2 = \left(1 - e^{\gamma_2 t}\right). \tag{6.62b}$$

Utilizing these expressions, the time evolution of the potential gradient and force free flow are

$$\frac{\partial \Phi}{\partial \rho}(t) = F_0 + F_1 T_1 + F_2 T_2, \tag{6.63}$$

$$\lambda(t) = G_1 T_1 + G_2 T_2. \tag{6.64}$$

Note that G_1 and G_2 each have units of cm^2/(statVolt·sec), and F_0, F_1, and F_2 have units of 1/cm. The electric field and bootstrap flow each have a two time scale dependence.

These expressions can be used to calculate U^{ζ} and U^{α} using equations (6.6) and (6.7). After defining

$$V_1 = \left(\frac{cF_1}{B^{\zeta}\sqrt{g}} + B^{\alpha}G_1\right), \tag{6.65}$$

$$V_2 = \left(\frac{cF_2}{B^{\zeta}\sqrt{g}} + B^{\alpha}G_2\right). \tag{6.66}$$

the time dependence of the contravariant components of the flow can be written as:

$$U^{\alpha}(t) = V_1T_1 + V_2T_2, \tag{6.67}$$

$$U^{\zeta}(t) = B^{\zeta}G_1T_1 + B^{\zeta}G_2T_2. \tag{6.68}$$

The terms V_1, V_2, $B^{\zeta}G_1$, $B^{\zeta}G_2$ have units of 1/sec. It is also possible to break the flows into a component rising on the fast time scales and a component rising on a slow time scale. By using $\mathbf{U}=U^{\alpha}\mathbf{e}_{\alpha}+U^{\zeta}\mathbf{e}_{\zeta}$, the vector flow becomes

$$\mathbf{U}(t) = \left(V_1\mathbf{e}_{\alpha} + B^{\zeta}G_1\mathbf{e}_{\zeta}\right)T_1 + \left(V_2\mathbf{e}_{\alpha} + B^{\zeta}G_2\mathbf{e}_{\zeta}\right)T_2. \tag{6.69}$$

The first term in parenthesis represents the direction of the fast rising flow, and will be called the "fast direction". The second term represents the slow rising flow direction and is called the "slow direction".

The more HSX relevant use of this formulation involves the decay of the plasma flow and electric fields when the electrode current is abruptly terminated. Let the radial current be turned off at $t=t_0$, and call $\Phi_0'=\partial\Phi/\partial\rho(t=t_0)$ and $\lambda_o=\lambda(t=t_0)$. If the flows have been allowed to achieve steady state, then these quantities are simply given by $\lambda_o=G_1+G_2$ and $\Phi_0'=F_0+F_1+F_2$. The time evolution of the electric field and parallel flow for $t>t_o$ can be written as

$$\lambda(t) = N_4e^{\gamma_1(t-t_0)} + N_5e^{\gamma_2(t-t_0)}, \tag{6.70}$$

$$\frac{\partial\Phi}{\partial\rho}(t) = N_1e^{\gamma_1(t-t_0)} + N_2e^{\gamma_2(t-t_0)} + N_3, \tag{6.71}$$

where the following definitions have been used

$$N_1 = D_3 + \frac{D_1}{\gamma_1(\gamma_2 - \gamma_1)}, \tag{6.72a}$$

$$N_2 = D_4 + \frac{D_2}{\gamma_2(\gamma_2 - \gamma_1)}, \tag{6.72b}$$

$$N_3 = \frac{\gamma_2 D_1 + \gamma_1 D_2}{\gamma_1 \gamma_2 (\gamma_2 - \gamma_1)}, \tag{6.72c}$$

$$N_4 = \frac{D_1}{\gamma_1} \frac{\gamma_1 - d_{11}}{d_{12}(\gamma_2 - \gamma_1)} + \frac{D_3(\gamma_1 - d_{11})}{d_{12}}, \tag{6.72d}$$

$$N_5 = \frac{D_2}{\gamma_2} \frac{\gamma_2 - d_{11}}{d_{12}(\gamma_2 - \gamma_1)} + \frac{D_4(\gamma_2 - d_{11})}{d_{12}}, \tag{6.72e}$$

$$D_1 = (\gamma_2 - d_{11})S_1 - d_{12} S_2, \tag{6.72f}$$

$$D_2 = d_{12} S_2 - (\gamma_1 - d_{11})S_1, \tag{6.72g}$$

$$D_3 = \frac{1}{(\gamma_2 - \gamma_1)}\left[(\gamma_2 - d_{11})\Phi_0' - d_{12}\lambda_0\right], \tag{6.72h}$$

$$D_4 = \frac{1}{(\gamma_2 - \gamma_1)}\left[d_{12}\lambda_0 - (\gamma_1 - d_{11})\Phi_0'\right]. \tag{6.72i}$$

The terms S_1 and S_2 are evaluated with $\langle \mathbf{J}_{ext} \cdot \nabla\rho \rangle = 0$. With these definitions, the flow evolution at bias turn off can be written as

$$\mathbf{U}(t > t_0) = \left(N_4 \mathbf{B} + \frac{cN_1}{B^{\xi}\sqrt{g}} \mathbf{e}_{\alpha} \right) e^{\gamma_1 (t - t_0)} + \left(N_5 \mathbf{B} + \frac{cN_2}{B^{\xi}\sqrt{g}} \mathbf{e}_{\alpha} \right) e^{\gamma_2 (t - t_0)}, \tag{6.73}$$

As expected, the two decay time scales each have a direction associated with them. Further, it can be shown that the directions associated with the fast time scale are the same for the rise and the fall. In this sense, this direction can be considered the direction of fast flow change after an abrupt change in the electrode current. The same holds for the slow times scales, and the direction associated with the slow time scales can be considered the direction of slow change.

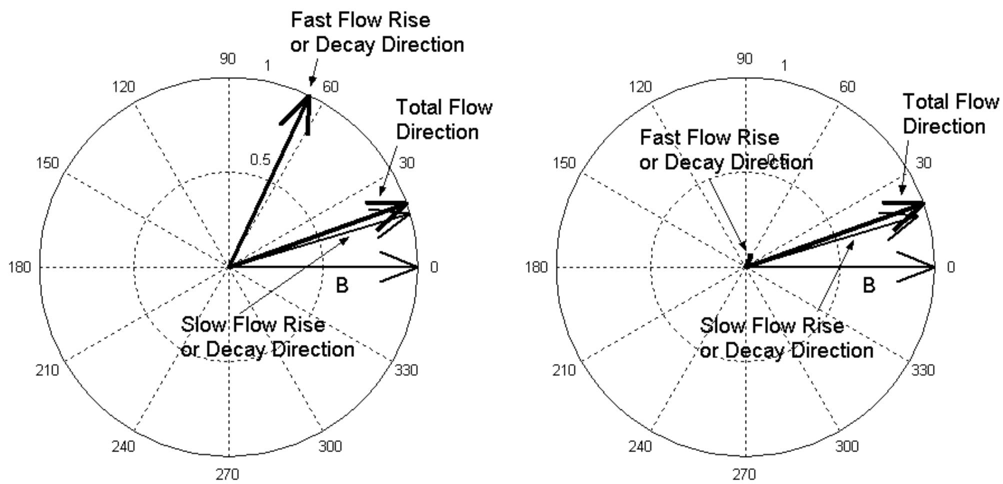

Figure 6.6 Directions of fast, slow, and total flow for the QHS configuration. All arrows normalized to unit length in the left frame, but with proper relative length in the right frame.

Figure 6.6 illustrates the directions associated with the two time scales in this model. The coordinate system in this figure lies in the plane of the flux surface, with the polar angle rotated such that the magnetic field points directly to the right. In making this calculation, the steady state quantities V_1, V_2, G_1, and G_2 were first calculated. These quantities, coupled with the numerically calculated covariant basis vectors, were used with equation (6.69) to project the predicted flows into physical space. The calculation is done at the location between coils 1 and 2, where the low field side Mach probe resides. The calculations are for the QHS case with a neutral density of $1\text{x}10^{10}$ cm^{-3}, a value appropriate for the experimental conditions.

The graph on the left shows the neoclassical fast and slow directions with all of the arrows normalized to unit length. The graph on the right shows the same directions, but with the proper relative lengths. This illustrates that most of the flow is predicted to be in the slow direction in the QHS case. The fast and flow directions are insensitive to the neutral density in this regime, although the amount of flow in each of the two directions changes with the neutral density.

The graph shows the neoclassical predictions for the fast and slow flow, illustrating that most of the flow is predicted to be in the slow direction in the QHS case. The fast and flow directions are insensitive to the neutral density in this regime, although the amount of flow in the two directions changes with the neutral density.

It is interesting to compare the neoclassical slow direction to the direction of symmetry in the (n,m)=(4,1) component of the field. This symmetry direction can be found by writing the single term Fourier expansion of |B| in Hamada coordinates:

$$B = B_o\left(1 + b_{m,n}\cos(n\zeta - m\alpha)\right) \tag{6.74}$$

where n=4 and m=1 denote that only the main helical component is under consideration. Taking the gradient of (6.74) yields the direction on a flux surface of greatest change in |B|:

$$\nabla B = -B_o b_{m,n}\cos(n\zeta - m\alpha)\left[-m\nabla\alpha + n\nabla\zeta\right]. \tag{6.75}$$

The direction of symmetry can be found by crossing ∇B with $\nabla\rho$.

$$\nabla B \times \nabla\rho = -B_o b_{m,n}\cos(n\zeta - m\alpha)\left[-m(\nabla\alpha \times \nabla\rho) + n(\nabla\zeta \times \nabla\rho)\right]. \tag{6.76}$$

The relationship between the contravariant and covariant basis vectors, equation (5.4), can be used to derive

$$\nabla B \times \nabla\rho = B_o b_{m,n}\cos(n\zeta - m\alpha)\left[m\mathbf{e}_\zeta + n\mathbf{e}_\alpha\right]. \tag{6.77}$$

This direction can be written in terms of the Hamada toroidal and poloidal fields as

$$\nabla B \times \nabla\rho = B_o b_{m,n}\cos(n\zeta - m\alpha)\left[m\frac{\mathbf{B}_T}{B^\zeta} + n\frac{\mathbf{B}_P}{B^\alpha}\right]. \tag{6.78}$$

After factoring out a factor of $1/B^\alpha$ and neglecting the material in front of the brackets, the direction of symmetry can be written as

$$\mathbf{s} = ɨm\mathbf{B}_T + n\mathbf{B}_P, \tag{6.79}$$

With the knowledge of the Hamada basis vectors, this direction can be calculated in real space in the same manner that the real space flows were calculated.

The slow flow change direction is plotted against the symmetry direction in figure 6.7. The figure illustrates quite clearly that the direction of symmetry and the direction of slow flow change are exactly parallel to each other.

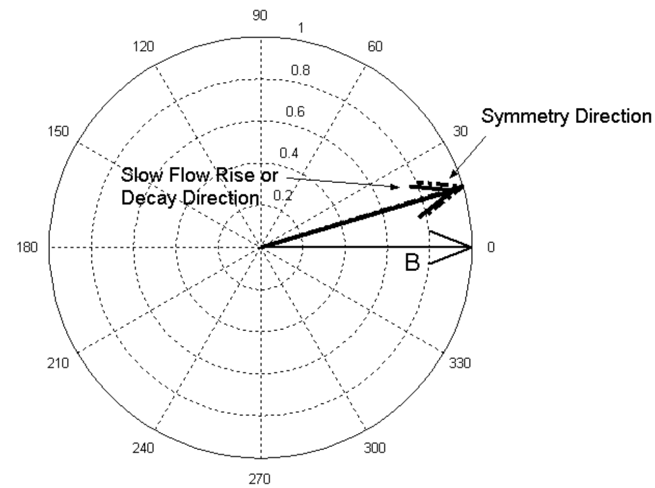

Figure 6.7 Comparison between the direction of slow flow change and the direction of symmetry.

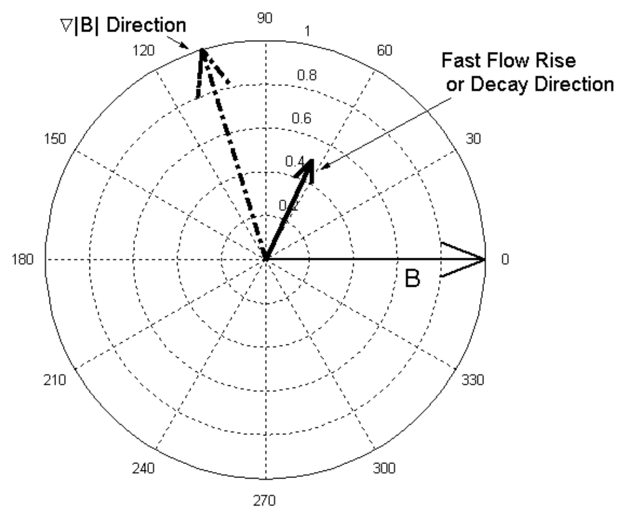

Figure 6.8 Comparison between the direction of fast flow change and the direction of ∇|B| on a flux surface.

A comparison between the direction of fast flow change and the direction of ∇B is illustrated in figure 6.8. The lengths of the vectors have been chosen so that they appear visibly on the plot; only the directions of these vectors should be considered. These two directions do not coincide. Consider that there are flows across the direction of symmetry that are damped on a fast time scale. To maintain incompressibility, these flows must be accompanied by Pfirsch-Schlueter type parallel flows. Furthermore, the time changing electric field will lead to some change in the force free parallel flow, as indicated by the parallel momentum balance in equation 6.1. Hence, all of the relevant flow mechanisms are changing on a fast time scale, leading to the total direction for the fast changing flows illustrated in figure 6.8.

A calculation of the fast and slow damping rates for the QHS configuration will be given at the end of the next section, after a final time scale is introduced.

6.4.3 "Forced E_r" Model.

The Coronado and Talmadge model appears to be representative of the relaxation phase in the HSX experiments, when the abrupt termination of the electrode current initiates the decay of the plasma flows and electric field. As was discussed in Chapter 4, the electric field formation/spin-up phase appears to be governed by different dynamics. The electric field goes to its steady state value very quickly, while the electrode current has a large transient before settling down to its steady state value. These observations have motivated the original modeling which is the subject of this subsection.

To model the spin-up of the plasma, assume that the potential gradient $\partial\Phi/\partial\rho$ changes very quickly, in a way specified before the equations are solved, i.e. that $\partial\Phi/\partial\rho$ and $(\partial/\partial t)(\partial\Phi/\partial\rho)$ are both known as a function of time. The parallel momentum balance equation can be cast as an equation for the evolution of λ as

$$a_4 \frac{\partial \lambda_i}{\partial t} + b_4 \lambda_i = C_2 - a_3 \frac{\partial}{\partial t}\frac{\partial \Phi}{\partial \rho} - b_3 \frac{\partial \Phi}{\partial \rho}, \tag{6.80}$$

The equation can be solved in general as

$$\lambda(t) = \mathbf{exp}\left(-\frac{b_4}{a_4}t\right)\left(\int \mathbf{exp}\left(\frac{b_4}{a_4}t\right)\left(C_2 - a_3\frac{\partial}{\partial t}\frac{\partial\Phi}{\partial\rho} - b_3\frac{\partial\Phi}{\partial\rho}\right)dt + \text{Const.}\right), \tag{6.81}$$

subject to the initial condition that $\lambda(t=0)=0$. This integral can be solved analytically for simple models of the potential gradient evolution, or the differential equation can be solved numerically if necessary. Once this equation has been solved, the contravariant components of the velocity can be determined from (6.6) and (6.7). With the knowledge of the Hamada coordinate system, the lab frame flow velocity can be determined. Once λ and $\partial\lambda/\partial t$ are known from the parallel momentum balance, the external current can be specified through the poloidal momentum balance as:

$$< \mathbf{J}_{ext}\cdot\nabla\rho >= \left[\begin{array}{l} a_1\frac{\partial}{\partial t}\frac{\partial\Phi}{\partial\rho} + a_2\frac{\partial\lambda_i}{\partial t} + b_1\frac{\partial\Phi}{\partial\rho} + b_2\lambda + \\ \frac{1}{eN_i}\frac{\partial p_i}{\partial\rho}\left(\upsilon_\alpha^{(P)} + \upsilon_{in}\frac{\langle f_n(\alpha,\zeta)\mathbf{B}_P\cdot\mathbf{B}_P\rangle}{\langle\mathbf{B}_P\cdot\mathbf{B}_P\rangle}\right)\end{array}\right] * m_i N_i < B_P^2 > \left(\frac{c}{\sqrt{g}B^\alpha B^\varsigma}\right)^2. \tag{6.82}$$

As a simple example of an analytic solution to these equations, a potential gradient evolution can be specified as

$$\frac{\partial\Phi}{\partial\rho} = \begin{cases} E_{r0} = \dfrac{-1}{eN_i}\dfrac{\partial p_i}{\partial\rho} & t<0 \\ E_{r0} + \kappa_E\left(1-e^{-t/\tau}\right) & t>0 \end{cases}. \tag{6.83}$$

The potential gradient for t<0 is set to balance the pressure gradient, as described in Section 6.1. The growth time of the potential gradient is τ, and should be set very fast ($\approx$1 μs for the HSX electrode system). The increase in the potential gradient at steady state is given by κ_E (units of 1/cm), and is a free parameter in the model. This function can be differentiated to yield.

$$\frac{\partial}{\partial t}\frac{\partial\Phi}{\partial\rho} = \begin{cases} 0 & t<0 \\ \dfrac{\kappa_E}{\tau}e^{-t/\tau} & t>0 \end{cases}. \tag{6.84}$$

Plugging these expressions into the differential equation for λ yields an equation of the form

$$a_4 \frac{d\lambda}{dt} + b_4\lambda = C_2 - b_3\left(E_{r0} + \kappa_E\right) + e^{-t/\tau}\kappa_E\left(b_3 - a_3/\tau\right). \tag{6.85}$$

This differential equation can be written

$$\tilde{A}\frac{d\lambda}{dt} + \tilde{B}\lambda = \tilde{C} + \tilde{D}e^{-t/\tau}. \tag{6.86}$$

which has an analytic solution

$$\lambda(t) = \frac{\tilde{C}}{\tilde{B}}\left(1 - \left(1 + \frac{\tilde{B}\tilde{D}}{\tilde{C}\left(\tilde{B} - \frac{\tilde{A}}{\tau}\right)}\right)e^{-\frac{\tilde{B}}{\tilde{A}}t} + \frac{\tilde{B}\tilde{D}}{\tilde{C}\left(\tilde{B} - \frac{\tilde{A}}{\tau}\right)}e^{-t/\tau}\right). \tag{6.87}$$

After some algebra, it is possible to simplify this equation for the λ evolution to read

$$\lambda(t) = \kappa_E Q_1\left(1 - \left(1 + Q_2\right)e^{-\upsilon_F t} + Q_2 e^{-t/\tau}\right). \tag{6.88}$$

The constants are defined in terms of the viscous frequencies and the ion-neutral collision frequency as

$$Q_1 = -\frac{c}{\sqrt{g}B^{\alpha}B^{\varsigma}}\frac{t\upsilon_{\alpha} + \upsilon_{in0}\frac{\left\langle f_n(\alpha,\zeta)\mathbf{B}\cdot\mathbf{B}_p\right\rangle}{\left\langle B^2\right\rangle}}{t\upsilon_{\alpha} + \upsilon_{\zeta} + \upsilon_{in0}\frac{\left\langle f_n(\alpha,\zeta)B^2\right\rangle}{\left\langle B^2\right\rangle}}, \tag{6.89a}$$

$$Q_2 = \frac{\dfrac{\left(\iota\upsilon_\alpha + \upsilon_\zeta + \upsilon_{in0}\dfrac{\langle f_n(\alpha,\zeta)\mathbf{B}\cdot\mathbf{B}\rangle}{\langle B^2\rangle}\right)}{\left(\iota\upsilon_\alpha + \upsilon_{in0}\dfrac{\langle f_n(\alpha,\zeta)\mathbf{B}\cdot\mathbf{B}_p\rangle}{\langle B^2\rangle}\right)}\times\left(\iota\upsilon_\alpha + \dfrac{1}{\langle B^2\rangle}\left(\upsilon_{in0}\langle f_n(\alpha,\zeta)\mathbf{B}\cdot\mathbf{B}_p\rangle - \dfrac{\langle\mathbf{B}\cdot\mathbf{B}_p\rangle}{\tau}\right)\right)}{\left(\iota\upsilon_\alpha + \upsilon_\zeta + \upsilon_{in0}\dfrac{\langle f_n(\alpha,\zeta)\mathbf{B}\cdot\mathbf{B}\rangle}{\langle B^2\rangle} - \dfrac{1}{\tau}\right)}, \tag{6.89b}$$

$$\upsilon_F = \frac{b_4}{a_4} = \iota\upsilon_\alpha + \upsilon_\zeta + \upsilon_{in0}\frac{\langle f_n(\alpha,\zeta)\mathbf{B}\cdot\mathbf{B}\rangle}{\langle B^2\rangle}. \tag{6.90}$$

Q_1 has units of cm^3/(statVolt·sec), while Q_2 is dimensionless and ν_F has units of 1/sec. In general, the quantity Q_2 is much less than one.

Based on this analytic solution for λ, the flow evolution for t>0 can be calculated as

$$U^\zeta(t) = B^\zeta\kappa_E Q_1\left(1-(1+Q_2)e^{-\upsilon_F t} + Q_2 e^{-t/\tau}\right), \tag{6.91}$$

$$U^\alpha(t) = U_E^\alpha\left(1-e^{-t/\tau}\right) + B^\alpha Q_1\kappa_E\left(1-(1+Q_2)e^{-\upsilon_F t} + Q_2 e^{-t/\tau}\right). \tag{6.92}$$

In this equation, the fast change in the poloidal flow due to the electric field increment is given by

$$U_E^\alpha = \frac{c}{B^\zeta\sqrt{g}}\kappa_E. \tag{6.93}$$

Having written the contravariant components of the flow in this simplified form, the vector flow can be written simply as

$$\mathbf{U}(t) = U_E^\alpha\left(1-e^{-t/\tau}\right)\mathbf{e}_\alpha + \mathbf{B}Q_1\kappa_E\left(1-(1+Q_2)e^{-\upsilon_F t} + Q_2 e^{-t/\tau}\right). \tag{6.94}$$

An analytic form for the external radial current can be derived from the poloidal force balance. By defining a further set of constants

$$Q_3 = m_i N_i < B_P^2 > \left(\frac{c}{\sqrt{g} B^\alpha B^\varsigma} \right)^2 \kappa_E \left\{ a_1 \frac{1}{\tau} - Q_1 Q_2 \frac{a_2}{\tau} + b_2 Q_1 Q_2 - b_1 \right\}, \quad (6.95a)$$

$$Q_4 = m_i N_i < B_P^2 > \left(\frac{c}{\sqrt{g} B^\alpha B^\varsigma} \right)^2 \kappa_E \left\{ a_2 Q_1 \upsilon_F (1 + Q_2) - b_2 Q_1 (1 + Q_2) \right\}, \quad (6.95b)$$

$$Q_5 = m_i N_i < B_P^2 > \left(\frac{c}{\sqrt{g} B^\alpha B^\varsigma} \right)^2 \kappa_E \left\{ b_1 + b_2 Q_1 \right\}, \quad (6.95c)$$

the external current can be calculated as

$$< \mathbf{J}_{ext} \cdot \nabla\rho >= Q_3 e^{-t/\tau} + Q_4 e^{-\upsilon_F t} + Q_5 . \quad (6.96)$$

At steady state, the electric field increment is related to the external current through the expression

$$< \mathbf{J}_{ext} \cdot \nabla\rho >_{ss} = \kappa_E m_i N_i < B_P^2 > \left(\frac{c}{\sqrt{g} B^\alpha B^\varsigma} \right)^2 \left(\begin{array}{c} \upsilon_\alpha^{(P)} + \upsilon_{in0} \dfrac{\left\langle f_n(\alpha,\zeta) \vec{B}_P \cdot \vec{B}_p \right\rangle}{\left\langle B_p^2 \right\rangle} - \\ \left(\dfrac{\upsilon_\alpha^{(P)} + q\upsilon_\varsigma^{(P)} + \upsilon_{in0} \dfrac{\left\langle f_n(\alpha,\zeta) \vec{B} \cdot \vec{B}_p \right\rangle}{\left\langle B_p^2 \right\rangle}}{\iota\upsilon_\alpha + \upsilon_\zeta + \upsilon_{in0} \dfrac{\left\langle f_n(\alpha,\zeta) \vec{B} \cdot \vec{B} \right\rangle}{\left\langle B^2 \right\rangle}} \right) \times \\ \left(\iota\upsilon_\alpha + \upsilon_{in0} \dfrac{\left\langle f_n(\alpha,\zeta) \vec{B} \cdot \vec{B}_p \right\rangle}{\left\langle B^2 \right\rangle} \right) \end{array} \right) \quad (6.97)$$

6.4.4 Comparison and Synthesis of the Two Models.

A calculation of the three different damping rates (γ_1,γ_2, and ν_F) for the QHS configuration is shown in figure 6.9, where the neutral density has been set to zero. The damping in this plot is solely due to symmetry breaking ripples in the magnetic field. All other parameters in the calculation are similar to those realized in experiments in HSX.

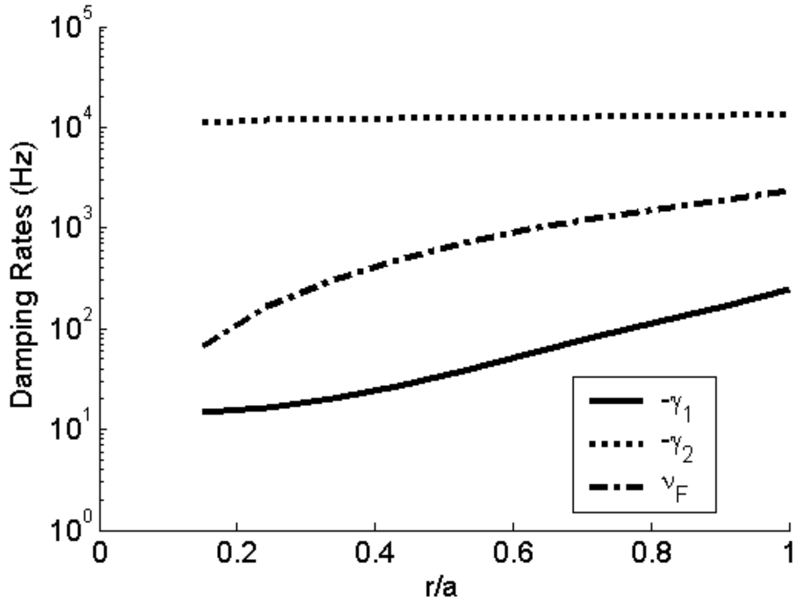

Figure 6.9: The three damping rates γ_1, γ_2, and ν_F, for the QHS configuration.

The slow neoclassical damping rate (γ_1) is from two to three orders of magnitude slower than the fast neoclassical damping rate (γ_2). The forced response rate, ν_F, is intermediate to the two rates. This rate contains information about damping both along and across the direction of symmetry.

An interpretations of the relationship between the three different time scales (γ_1, γ_2, and ν_F) is as follows. There are two variables necessary to define the neoclassical response on a flux surface, because the flux surface is a two dimensional structure. Possible choices for these variables include any two of the contravariant flow speeds U^α and U^ξ, the "bootstrap flow" λ, and the potential gradient $\partial\Phi/\partial\rho$. These variables appear in the time derivatives in the momentum equations. In the spin-down solution, the external current is shut off. This represents a change in the driving term, and two time scales are observed. These time scales and directions are the "normal modes" of the system, as evident in the eigenvalue solution surrounding equation (6.60). For the flow rise solution, one of the inherent system variables ($\partial\Phi/\partial\rho$) is externally driven by the electrode turn on. There is only one time scale left for the system to respond with; this time scale is thus a hybrid of the normal modes of the system.

An example of the time evolution of the flux surface quantities is shown in figure 6.10. The calculation is for the QHS case, on a surface at r/a≈0.75, assuming an electrode current of 7.5 A in steady state. The "Forced-E_r" model is used to model the evolution of the plasma when the electrode voltage is applied, while the Coronado and Talmadge formulation is applied to the plasma relaxation. The most important features to observe are the asymmetries between the rise and decay of the various quantities. This asymmetry mirrors that in the measurements. As an example, note the similarities in the external current evolution in this figure and the measurement in figure 4.23.

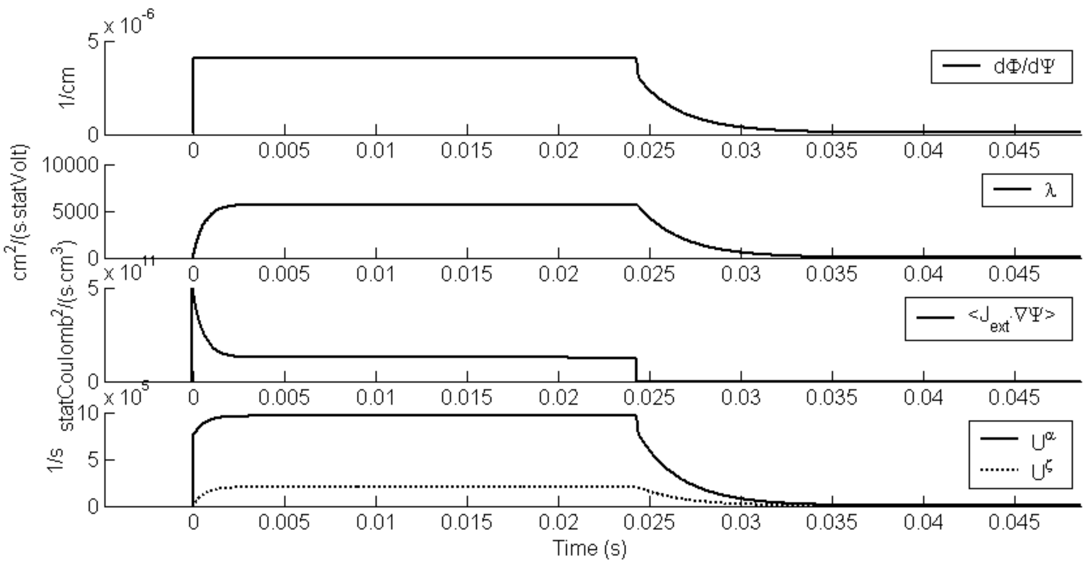

Figure 6.10 The evolution of the flux surface quantities throughout a 25ms long bias pulse.

As a caveat, it should be noted that the modeling assumes a pure electron-proton plasma. It is not clear to what extent this approximation holds in HSX. In discharges where probes are inserted too far into the plasma and density control is lost, substantial boron contamination of the plasma is known to occur. While the density was well controlled during the discharges in this dissertation, there may be some boron or other impurities contaminating the plasma. In general, the Z_{eff}=1 approximation may not be fully appropriate for HSX plasmas.

6.5: A Comparison of Viscous Damping in the QHS and 10% Mirror Configurations.

To finish this chapter, a brief comparison between the 10% Mirror and QHS configurations is provided. These two configurations are special, in that nearly all of the data in this dissertation was taken in these two configurations. The theory/experiment comparisons in Chapter 7 will concentrate on these two cases. Detailed calculations of the viscous damping in other configurations of HSX are to be found in Appendix 5.

These calculations are done with the neutral density set to zero, so that the differences in neoclassical viscous damping between the two configurations are most apparent. The other parameters in the calculation are similar to those in the experiment.

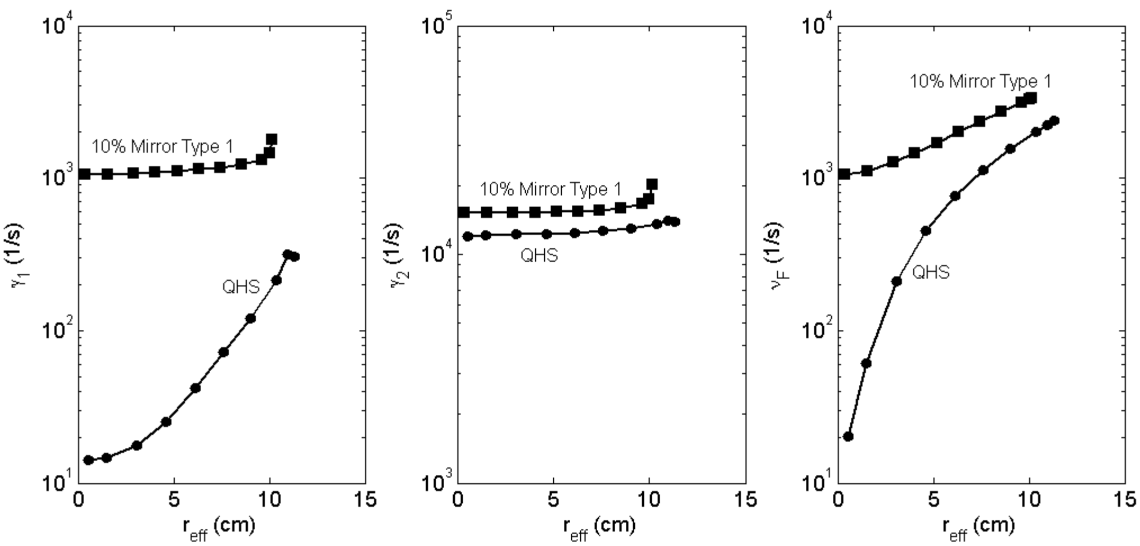

Figure 6.11 Comparison of the viscous damping time scales between the QHS and 10% Mirror configurations. Note the different scales.

The slower damping rate (γ_1) is shown in the left frame of figure 6.11. The difference in the slow damping rate is approximately two orders of magnitude in the core, and is reduced to a factor of 5-10 towards the edge. The large difference in this time scale is due to the (n,m)=(4,0) symmetry breaking term in the magnetic field spectrum of the Mirror configuration.

The faster damping rate (γ_2) is illustrated in the center frame of the figure. The difference between the two configurations is not large. This illustrates that the damping of flows across the direction of symmetry is comparable for the two cases.

The hybrid rate (ν_F) is illustrated in the right frame. The difference between the hybrid rates is larger than the difference between the fast rates, but smaller than the difference between the slow rates. Towards the edge, the difference in this ν_F between the two configurations is about a factor of 2. This is approximately the difference in the slow flow rise rates illustrated in Section 4.5.

6.6: Summary

The neoclassical damping formalism has been presented in detail in this chapter. The method involves simultaneously solving two projections of the momentum balance equation on a flux surface. Neoclassical parallel viscosity and ion-neutral friction (with toroidally asymmetric neutrals) are allowed as damping mechanisms. Steady state solutions of the fluid equations are found, leading to the neoclassical prediction of the radial conductivity.

To model the spin-up of the plasma when the electrode voltage is applied, we assume that the electric field is quickly applied to the plasma. This assumption is based on experimental observations, and leads to the result that the **E**x**B** and compensating Pfirsch-Schlueter like flows grow on the same time scale of the electrode voltage. The bootstrap-like component of the parallel flow grows on a hybrid time scale which involves the damping rates in the toroidal and poloidal directions.

At electrode bias turn off, the external current is broken and the electrode voltage is allowed to decay. Modeling this leads to a two time scale flow decay; the two time scales correspond to two directions on a flux surface. It was shown that the while the slow time scale corresponds to the damping of flows along the direction of symmetry. The fast time scale corresponds to the damping of flows across the direction of symmetry, as well as the accompanying Pfirsch-Schlueter and force-free flows.

[1] M. Coronado and J. N. Talmadge, Phys. Fluids B **5**, 1200 (1993).

[2] J.D. Callen, NEEP 903 Notes. U. of Wisconsin-Madison (1986)

[3] M. Coronado and H. Wobig, Phys. Fluids **29**, 527 (1986).

[4] K.C. Shaing and J.D. Callen, Phys. Fluids **26**, 3315 (1983).

[5] K. C. Shaing, S.P. Hirshman, and J.D. Callen, Phys. Fluids **29**, 521 (1986).

[6] M. Okabayashi and S. Yoshikawa, Phys. Rev. Lett. **29**, 1725 (1972).

[7] J.N. Talmadge, B.J. Peterson, D.T. Anderson, F.S.B. Anderson, H. Dahi, J.L. Shohet, M. Coronado, K.C. Shaing, et. al., Proceedings of the 15th International Conference on Plasma Physics and Controlled Fusion Research (Seville, 1994), IAEA, Vienna, **1** (1995) 797.

[8] M. Coronado and H. Wobig, Phys. Fluids **30**, 3171 (1987).

[9] R.K.Janeev, W.D. Langer, K. Evans, Jr., and D.E. Post, Jr., *Elementary Processes in Hydrogen-Helium Plasmas*, (Springer, Berlin, 1987).

[10] G.S. Voronov, ATOMIC DATA AND NUCLEAR DATA TABLES **57**, 11, (1994).

[11] W. Lotz, Astrophys. J. Supplement. Series **14**, 207 (1967).

[12] R.L. Freeman and E.M. Jones, Atomic Collision Processes in Plasma Physics Experiments, CLM-R 137, UKAEA Research Group, 1974.

[13] Heifetz, D.B. et. al., J. Comp. Phys. **46,** 309 (1982).

[14] W.E. Boyce and R.C. DiPrima, *Elementary Differential Equations and Boundary Value Problems*, (John Wiley & Sons, New York, 1992), p. 17.